Environmental Science & Technology

Article

pubs.acs.org/est

Complex Refractive Indices of Thin Films of Secondary Organic Materials by Spectroscopic Ellipsometry from 220 to 1200 nm

Pengfei Liu,[†] Yue Zhang,[†] and Scot T. Martin*[,†,‡]

[†]School of Engineering and Applied Sciences, Harvard University, Cambridge, Massachusetts 02138, United States

[‡]Department of Earth and Planetary Sciences, Harvard University, Cambridge, Massachusetts 02138, United States

Supporting Information

ABSTRACT: The complex refractive indices of three different types of secondary organic material (SOM) were obtained for 220 to 1200 nm using a variable angle spectroscopic ellipsometer. Aerosol particles were produced in a flow tube reactor by ozonolysis of volatile organic compounds, including the monoterpenes α-pinene and limonene and the aromatic catechol (benzene-1,2-diol). Optically reflective thin films of SOM were grown by electrostatic precipitation of the aerosol particles onto silicon substrates. The ellipsometry analysis showed that both the real and imaginary components of the refractive indices decreased with increasing wavelength. The real part $n(\lambda)$ could be parametrized by the three-term form of Cauchy's equation, as follows: $n(\lambda) = B + C/\lambda^2 + D/\lambda^4$ where λ is the wavelength and B, C, and D are fitting parameters. The real refractive indices of the three SOMs ranged from 1.53 to 1.58, 1.49−1.52, and 1.48−1.50 at 310, 550, and 1000 nm, respectively. The catechol-derived SOM absorbed light in the ultraviolet (UV) range. By comparison, the UV absorption of the monoterpene-derived SOMs was negligible. On the basis of the measured refractive indices, optical properties were modeled for a typical atmospheric particle population. The results suggest that the wavelength dependence of the refractive indices can vary the Angstrom exponent by up to 0.1 across the range 310 to 550 nm. The modeled single-scattering albedo can likewise vary from 0.97 to 0.85 at 310 nm (UV−B). Variability in the optical properties of different types of SOMs can imply important differences in the relative effects of atmospheric particles on tropospheric photochemistry, as well as possible inaccuracies in some satellite-retrieved properties such as optical depth and mode diameter.

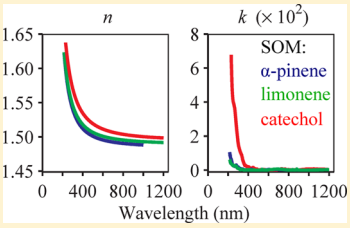

1. INTRODUCTION

Aerosol particles directly influence Earth's radiative balance by scattering and absorbing solar radiation. The particle optical properties quantifying this interaction with radiation, such as optical depth (AOD), single-scattering albedo (SSA), and phase function, are wavelength dependent. Although satellite remote sensing is able to provide global coverage of some of these properties,[1] the accuracy of retrieval algorithms depends in large part on the accuracy of the particle optical properties in those algorithms, both in the ultraviolet and visible portions of the spectrum. A lack of detailed knowledge concerning the wavelength-dependent optical properties induces uncertainties in satellite retrievals and hence assessments of the effects of atmospheric particles on climate forcing[2] and tropospheric photochemistry.[3]

Optical properties used in common retrieval algorithms are taken from databases and are therefore implicitly assumed as known values.[4,5] The databases are derived from microphysical particle parameters, typically by using Mie theory in conjunction with the complex refractive index m (i.e., $m = n - i\,k$ for refractory part n and absorptive part k) of the particle material and the number−diameter distribution of the particle population.[5,6] The database of microphysical parameters, especially the wavelength dependence of $m(\lambda)$, is incomplete and not fully representative of the variable particle composition found in the atmosphere. The present study focuses on measurements of $m(\lambda)$ for an important class of organic particles.

Secondary organic material (SOM) is a substantial, even dominant, fraction of the mass concentration of the submicrometer atmospheric particle population for many locations and times worldwide.[7] The direct radiative effect of this particle class is estimated as −0.08 to −0.78 W m^{-2}.[8] The accuracy of this model estimate is largely influenced by the assumed particle optical properties. Organic particles treated as nonabsorbing increase the total-sky and clear-sky top-of-atmosphere forcing by 47% and 18%, respectively.[9] A change in the real refractive index n from 1.4 to 1.5 for nonabsorbing particles is estimated to increase radiative forcing by 12% and likewise to decrease surface-level irradiation.[10] The absorptive component k can also be important for some types of SOM, both in the ultraviolet (UV) and visible.[11−13] Absorption by nitrated and aromatic molecules can significantly decrease UV irradiation of the atmospheric boundary layer.[14] Brown carbon can be produced by reactions of SOM with ammonia[13,15] and can decrease UV irradiation.[16,17] Changed irradiance has the potential to shift dominant reactions pathways for tropospheric

Received: August 1, 2013
Revised: November 3, 2013
Accepted: November 5, 2013
Published: November 5, 2013

chemistry by changing photolysis rates and production rates of many radical species.[14,18]

Given the importance of SOM and its optical properties, several laboratory studies have focused on this topic. SOM absorptive properties were characterized by collection of the absorbance spectra using a UV−visible spectrophotometer.[11−13,19,20] Refractory information (i.e., n) was not obtained by this approach. Measurements of extinction and scattering coefficients by cavity ring down spectroscopy and nephelometry, combined with knowledge of the number−diameter distribution of the particle population, were used to retrieve m, though only for specific wavelengths.[10,20−25]

Herein, spectroscopic ellipsometry[26] is introduced for the measurement of the wavelength-dependent complex refractive indices $m(\lambda)$ of secondary organic materials. Outside the atmospheric sciences, this technique has been applied in the study of the optical properties of organic polymer materials.[27,28] Within the atmospheric sciences, it has been applied to characterizing the interaction of hydrogen chloride with ice surfaces.[29] The technical challenge for the present study was the synthesis of optically reflective SOM films, as required for spectroscopic ellipsometry. Once grown, the m values of these films were obtained using variable angle spectroscopic ellipsometry from ultraviolet (220 nm) through visible to near-infrared (1200 nm) wavelengths. This spectral range is needed for atmospheric modeling and satellite remote sensing. Different types of SOM, representing clean and polluted conditions, were produced by ozonolysis of α-pinene, limonene, and catechol.[11,30]

2. EXPERIMENTAL SECTION

2.1. Production of Secondary Organic Material. Secondary organic material was produced by the ozonolysis of precursor compounds in a flow tube reactor (Figure 1). The experimental conditions are listed in Table 1. The flow tube was operated at a temperature of 298 ± 1 K, the relative humidity was below 5%, and the average retention time was 38 ± 1 s. Further technical information on the flow tube reactor appears in Shrestha et al.[31]

Ozone was produced outside the flow tube by irradiating pure air (Aadco 737 Pure Air Generator) with ultraviolet emissions of a mercury lamp. The ozone-to-hydrocarbon ratio exceeded 10:1, meaning that, the reactions were conducted in a condition of excess ozone. No NO_x was injected into the flow tube. The NO concentration in the pure air was below the detection limit (70 ppt) of the NO_x analyzer (Eco physics, CLD 899 Y).[32]

(−)-α-Pinene (Sigma Aldrich, ≥ 99%) and D-limonene (Sigma Aldrich, ≥ 97%) were dissolved in 2-butanol (Sigma Aldrich, ≥ 99.5%) at 2% solution (v/v). The organic solution was continuously injected using a syringe pump into a glass bulb and vaporized at 410 K. The vapors were swept into the flow tube where ozonolysis took place to produce a particle population. In control experiments using neat butanol, no particles were detected. During ozonolysis, hydroxyl (OH) radicals were produced by some reaction channels, and butanol served as an OH radical scavenger. Previous studies report that the presence of the OH scavenger has no discernible effect on the refractive indices of SOMs produced from α-pinene or limonene ozonolysis.[10,21]

For the ozonolysis of catechol, the solid precursor was dissolved to prepare a 25% (w/w) solution in ultrapure water. This solution was injected into a glass bulb using a syringe pump, vaporized at 553 K, and swept into the flow tube. In a control experiment for catechol without ozone, the particle mass concentration was 0.05% of that obtained in the presence of ozone, indicating that observed particle mass concentrations resulted from the condensation of oxidation products rather than catechol vapor.

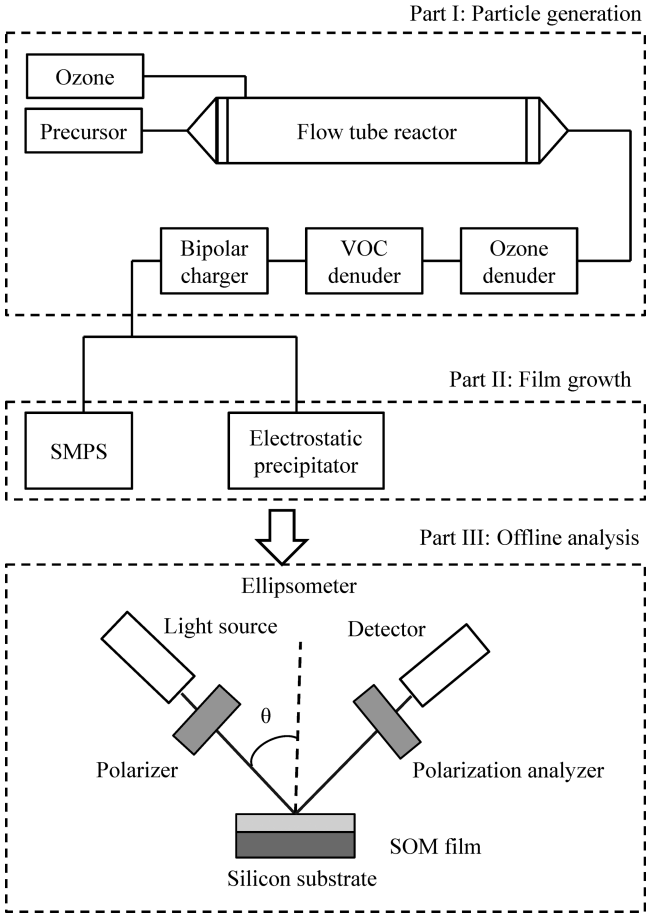

Figure 1. Schematic diagram of experimental apparatus. (i) Production of secondary organic material in aerosol form. (ii) Growth of a film of secondary organic material by electrostatic precipitation of aerosol particles onto a silicon substrate. (iii) Measurement of the wavelength-dependent complex refractive indices $m(\lambda)$ of the SOM film.

For all experiments, the outflow from the flow tube was passed through denuders for ozone (Ozone Solutions, model ODS-2) and semivolatile organic vapors (carbon filter, Sunset Laboratory) for reducing excess reactants that can possibly induce artifacts in the sampling process. More than 99% of ozone was removed from the sampling flow by denuders. The number−diameter distributions, number concentrations, and mass concentrations of the produced particle populations were characterized by a Scanning Mobility Particle Sizer (SMPS, TSI 3071A) that sampled the outflow from the flow tube. A material density of 1200 kg m^{-3} was used in the calculation of particle mass concentration.

2.2. Film Growth. The SOM aerosol particles in the outflow from the flow tube reactor were passed through a bipolar charger (TSI, 3077) and deposited onto silicon substrates (University Wafer, prime grade, resistance 1−10 Ω·cm) using an electrostatic precipitator (TSI 3089)[33] (Figure 1). An electric field focused positively charged particles onto the silicon substrate to deposit and grow an organic film. The

dx.doi.org/10.1021/es403411e | Environ. Sci. Technol. 2013, 47, 13594−13601

Table 1. Experimental Conditions for Production of Secondary Organic Material in Aerosol Form and Subsequent SOM Film Growth by Electrostatic Precipitation of the Aerosol Particles onto a Silicon Substrate[a]

	precursor	precursor conc. (ppm)	ozone conc. (ppm)	SOM mass conc. (μg m^{-3})	volume mode diameter (nm)	sampling voltage (kV)	sampling time (h)	sampling flow rate (L min^{-1})	film thickness (nm)	collection efficiency (%)
A1	(−)α-pinene	5.0	51.5 ± 0.4	(1.64 ± 0.12) × 10^4	300	−9.8	21	1.0	373 ± 2	1.1
A2	(−)α-pinene	5.0	51.4 ± 0.4	(1.62 ± 0.12) × 10^4	289	−6.0	14	1.0	282 ± 2	1.1
A3	(−)α-pinene	4.0	50.5 ± 0.5	(1.26 ± 0.08) × 10^4	269	−6.0	24	1.0	590 ± 3	2.0
A4	(−)α-pinene	2.0	55.4 ± 0.5	(3.74 ± 0.28) × 10^3	181	−6.0	23	1.0	254 ± 3	3.0
B1	D-limonene	3.0	30.0 ± 0.5	(1.01 ± 0.04) × 10^4	181	−9.8	15	1.0	591 ± 3	3.9
C1	catechol	2.0	124 ± 1	(3.37 ± 0.16) × 10^2	85	−9.8	67	1.5	466 ± 7	13.9

[a]Values show the mean ±1 standard deviation during the sampling periods.

precipitator consisted of a grounded cylindrical housing having a central electrode target (2.54 cm diameter). The collection voltage (<10 kV) of the precipitator was varied to obtain smooth films for the different samples (cf. Table 1). The silicon substrate was mounted onto the electrode using adhesive tape. Silicon substrates were used because of their conductivity, which favored efficient collection by electrostatic precipitation, and their high refractive index, which was significantly different from that of the overlying SOM film and thus improved ellipsometric characterization of the latter. In a control experiment under the same condition of Experiment A1 (Table 1), SOM particles were removed by a quartz filter in the sampling line, and no visible film formed. This result indicates that the thin organic films resulted from the deposition of SOM particles rather than condensation of organic vapors.

The films of SOM produced by this technique had mirror-like reflective surfaces (Figure 2a) that were ideal for ellipsometry measurement. The optical microscopic image confirmed the formation of flat films (Figure 2b). The root-mean-square surface roughness was 0.3 nm, as measured by atomic force microscopy (AFM, Veeco Nanoman VS) (Figure 2c).

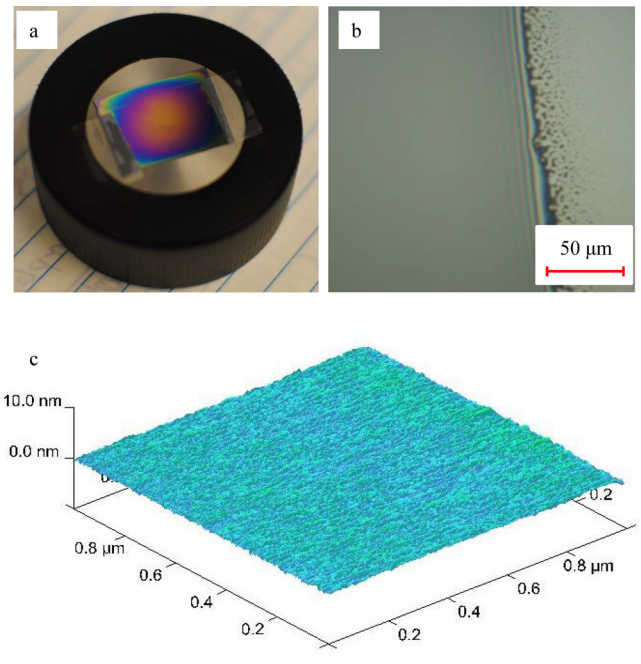

Figure 2. Film characterization. (a) Photograph of SOM film on silicon substrate. Apparent color arises from interference fringes of the visible light with the front and back surfaces of the film. (b) Image of SOM film as collected by optical microscopy (10×). The film is the left-hand side of the image. The right-hand side is the clean substrate after removal of the adhesive tape (cf. photograph in panel a). (c) Surface relief of SOM film as collected by tapping-mode atomic force microscopy.

2.3. Spectroscopic Ellipsometry. A variable angle spectroscopic ellipsometer (J.A. Woollam VASE) was used to characterize the optical properties of the SOM films. A broadband light source in the instrument covered 220 to 1200 nm (Figure 1). The instrument was equipped with a double monochromator for stray-light rejection and an autoretarder. The instrument was adjustable for a variable angle of incidence θ. In a typical measurement, the value of θ was scanned from 50 to 70° in steps of 5°. At each angle, the monochromator was scanned from 220 to 1200 nm in steps of 5 or 10 nm. At each θ–λ pair, the amplitude ratio and phase shift of reflected parallel p and perpendicular s polarized light from the surface were measured.

The raw data of ellipsometry measurements were the wavelength-dependent complex reflectance ratio $\rho(\lambda;\theta)$ of p- and s-polarized light from the surface at angle θ.[26] The ratio ρ is customarily expressed as $\rho = (\tan\psi)\exp(i\Delta)$, where $(\tan\psi)$ is the ratio of reflected amplitudes for the two polarizations and Δ is the relative phase shift. Because the primary measurement is a ratio, ellipsometry as a technique does not require an external reference, thereby favoring accuracy and reproducibility. The obtained data set $\rho(\lambda;\theta)$ was inverted to obtain $m(\lambda)$ values. The inversion analysis used an optical model for isotropic thin films with corrections for thickness nonuniformity. The commercially available WVASE32 software package (J.A. Woollam VASE) was used for the analysis.

Film thickness was also obtained as part of the inversion analysis. For the grown films, the thickness varied from 250 to 600 nm (Table 1). Best results are obtained from ellipsometry for film thickness approaching the wavelength of the light used in the measurements.[26] Ellipsometry also obtains best results for films of high uniformity and low surface roughness because inhomogeneities partially depolarize light upon light reflection. Depolarization of this kind can bias the data analysis.[26] In practical application, the film thickness must vary by no more than 10% over the sampling spot and the surface roughness must be less than 10% of the probe beam wavelength.[34] The SOM thin films synthesized from electrostatic precipitation in the present study, having a thickness nonuniformity of 3–10% over a sampling spot of 1–2 mm, met these requirements.

The collection efficiencies from particle population to film mass ranged from 1.1 to 13.9% for the different experiments (Table 1), as calculated by the ratio of the SOM film mass to the mass concentration in the flow multiplied by exposure time.

The collection efficiency was influenced both by the charging efficiency for positively charged particles and the efficacy of electrostatic precipitation. For the experimental conditions in this study, collection efficiency increased for particle populations of smaller mode diameters because the efficacy of electrostatic precipitation increased with the decreasing diameter.[33]

3. RESULTS AND DISCUSSION

3.1. Data Sets. The real and imaginary refractive indices measured for the different types of SOM are plotted in Figure 3. Results at 310 and 550 nm are summarized in Table 2.

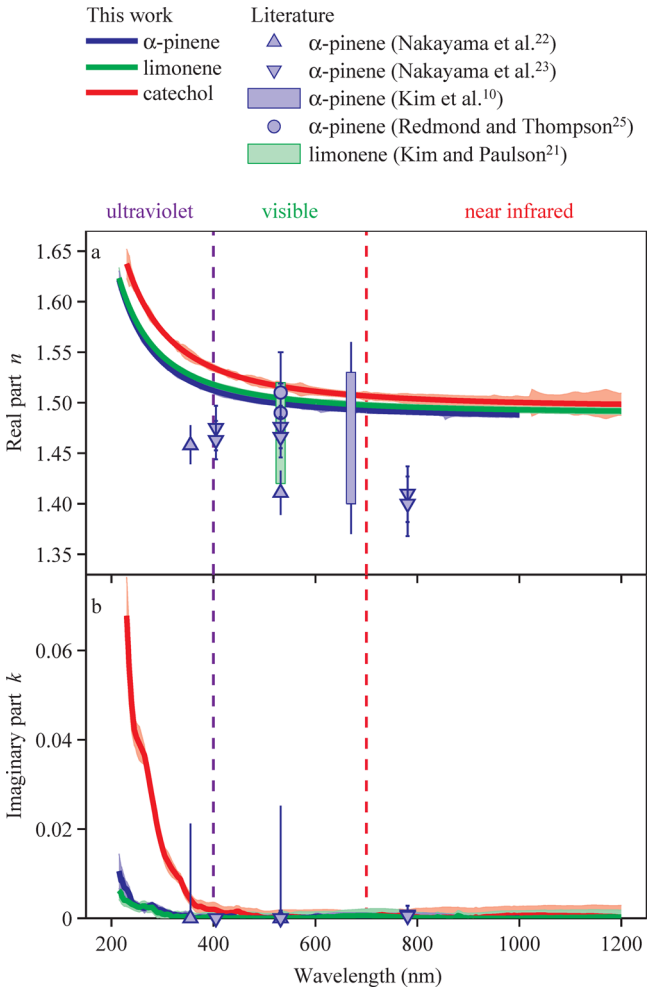

Figure 3. Wavelength-dependent complex refractive indices $m(\lambda)$ for different types of secondary organic material: (a) real part n and (b) imaginary part k. Results from literature are shown for comparison. The shading regions represent 10 and 90% confidence intervals estimated from fitting of ellipsometry data. The tabulated data of $m(\lambda)$ are provided in Supporting Information.

Variability in properties at 310 nm can affect atmospheric photochemistry. Variability in properties at 550 nm can influence the magnitude of the direct radiative effect and hence climate forcing. The real refractive indices n of α-pinene- and limonene-derived SOMs were 1.54 and 1.50 at 310 and 550 nm, respectively (Table 2). Catechol-derived SOM had higher n values of 1.57 and 1.52, respectively. The imaginary refractive indices k ($\times 10^4$) of the α-pinene-, limonene-, and catechol-derived SOMs at 310 nm were 12 ± 7, 9 ± 9, and 130 ± 20, respectively, indicating that the catechol-derived SOM was ten times more absorptive in the UV. The variability in refractive indices n among the different types of SOM stems from differences in chemical composition. Catechol-derived SOM has hydrogen to carbon (H:C) and oxygen to carbon (O:C) ratios of 1.0 and 0.3−1.0, respectively, while the H:C and O:C ratios for monoterpene-derived SOM are 1.4−1.6 and 0.3−0.6, respectively.[11,35,36] Predictive rules of refractive index can also be built up based on molecular formula[25] or functional groups,[37] although that information was absent for the present study.

Robustness of the obtained refractive indices was assessed by multiple experiments of α-pinene ozonolysis for different conditions and collection times that resulted in films of different thickness (Table 1, A1−A4; 250 to 600 nm thick). For these experiments, the absolute differences of retrieved refractive indices were within 0.01 for n and within 50×10^{-4} for k across 200 to 1200 nm. Within these same tolerances, the refractive indices did not depend on the mass concentration of the original particle population ($0.4-3.7 \times 10^4$ μg m^{-3} across experiments A1−A4).

For the studied SOMs, the real refractive indices n decreased with increasing wavelength (Figure 3a), meaning that they exhibited normal dispersion from the UV to the near-IR. The wavelength dependence was parametrized by a three-term form of Cauchy's equation:[38]

$$n(\lambda) = B + C/\lambda^2 + D/\lambda^4 \quad (1)$$

The fitting parameters B, C, and D for each SOM are listed in Table 3. The chromatic dispersion $\Delta n_{310,550}$ from UV−B (λ = 310 nm) to midvisible (λ = 550 nm) is also listed in Table 2 for each SOM, with high values indicating high dispersion. The Abbe number ζ, defined as $\zeta = (n_{587.56} - 1)/(n_{486.13} - n_{656.27})$, is also listed. Refractive indices $n_{587.56}$, $n_{486.13}$, and $n_{656.27}$ correspond to the Fraunhofer d-, F-, and C- spectral lines. The Abbe number is a measure of dispersion in the visible, with low values indicating high dispersion. The values of ζ and $\Delta n_{310,550}$ indicate that the wavelength dependence of the SOM measured in this study is stronger than that of some common atmospheric inorganic salts, such as sea salt, NH_4NO_3, and $(NH_4)_2SO_4$. Significant dispersion indicates that systematic errors in AOD calculations and retrievals can be introduced if the wavelength dependence of the real refractive index is omitted from models or algorithms.

For the studied SOMs, the imaginary refractive indices k were zero within measurement uncertainty at 550 nm, meaning that visible light absorption was negligible (Figure 3b). These values suggest that the studied SOMs are reflective in the visible and therefore that light absorption by these SOMs is typically not important for shortwave radiative transfer in the troposphere. In the UV, the k values increased for shorter wavelengths. At 310 nm, k approached 0.001 for the α-pinene- and limonene-derived SOMs and 0.01 for catechol-derived SOM. The weak and moderate absorption in the UV by these respective types of SOM indicate that the studied SOMs at sufficient mass concentrations in an atmospheric layer can absorb sufficient UV to perturb irradiance and thus alter the in situ photochemistry.

For comparison to the results of this study, literature data for SOM produced by ozonolysis in chamber experiments are also plotted in Figure 3. Most of the literature data are for α-pinene-derived SOM and are available only for specific wavelengths. The mass concentrations of SOM in those experiments ranged

Table 2. Complex Refractive Indices ($m = n - ik$) and Dispersion Parameters in the Ultraviolet (310 nm) and Visible (550 nm) for each SOM of this Study as well as for some Atmospherically Relevant Materials

	refractive indices				dispersion parameters	
material	n_{310}	n_{550}	k_{310}	k_{550}	$\Delta n_{310,550}$	ζ
α-pinene SOM[a]	1.536 ± 0.004	1.498 ± 0.002	$(12 \pm 7) \times 10^{-4}$	$1^{+4}_{-1} \times 10^{-4}$	0.038	58.3
limonene SOM[a]	1.542 ± 0.003	1.503 ± 0.003	$9^{+11}_{-9} \times 10^{-4}$	$0^{+11}_{-0} \times 10^{-4}$	0.038	55.9
catechol SOM[a]	1.565 ± 0.003	1.515 ± 0.004	$(13 \pm 2) \times 10^{-3}$	$4^{+15}_{-4} \times 10^{-4}$	0.050	41.5
dry sea salt[b]	1.508	1.495	1.4×10^{-6}	1.0×10^{-8}	0.014	52.7
dry NH_4NO_3[b]	1.572	1.556	1.4×10^{-8}	1.1×10^{-9}	0.016	140
dry $(NH_4)_2SO_4$[b]	1.549	1.530	1.0×10^{-7}	1.0×10^{-7}	0.019	63.1
water[b]	1.348	1.333	1.4×10^{-8}	2.0×10^{-9}	0.015	73.0

[a]This study. [b]Source: Lacis' Database (http://gacp.giss.nasa.gov/data_sets/). Uncertainties represent 10 and 90% confidence intervals estimated from fitting of ellipsometry data.

Table 3. Parameters for Cauchy's Equation (Eq 1) to Describe the Wavelength-Dependent Real Refractive Index n for the Different Types of Secondary Organic Materials of this Study[a]

Material	B	C (μm^2)	D (μm^4)
α-pinene SOM	1.4844	3.638×10^{-3}	1.248×10^{-4}
limonene SOM	1.4889	4.031×10^{-3}	1.009×10^{-4}
catechol SOM	1.4943	5.876×10^{-3}	0.896×10^{-4}

[a]Range of applicability is for 220 to 1200 nm.

from 100 to 1000 $\mu g\ m^{-3}$. The refractive indices were retrieved by inversion of in situ measurements of particle extinction, scattering, and absorption using measured particle number-diameter distributions in conjunction with Mie theory.[10,21−25] The accuracy of the inversions was limited in part by uncertainties in the optical and size measurements.[39] With these caveats in mind, the n values obtained in this study do not disagree with those of Redmond and Thompson,[25] Kim et al.,[10] and Kim and Paulson.[21] The n values reported by Nakayama et al.[22,23] are, however, somewhat lower than those of the present study. Even so, both studies report a decrease in n with increasing wavelength. The near-zero k values of the present study for 355 to 781 nm are also consistent with the results of Nakayama et al.[22,23] With respect to catechol-derived SOM, although refractive indices have not been reported in the literature, Ofner et al.[11] measured the UV−visible absorption spectrum and reported absorption up to 500 nm, in agreement with the present study.

The variation of n values among different studies for α-pinene- and limonene-derived SOMs can be caused in part by the differences in chemical composition, which is in turn influenced by experimental conditions, such as mass concentration, residence time, and so forth. Shilling et al.[40] observed that the elemental composition of α-pinene-derived SOM depends on mass concentration, although the dependence became weak for mass concentrations above 100 $\mu g\ m^{-3}$. Lambe et al.[20] demonstrated that the value of n decreased for increasing oxidation, at least for the studied SOM types. In the present study, the collection of sufficient quantities of SOM as needed for film growth implied the use of high mass concentrations (e.g., 3700−16000 $\mu g\ m^{-3}$ for α-pinene-derived SOM), corresponding to an order of magnitude greater than used in the comparative chamber experiments.[10,21−23] The low oxidation level which is typically associated with high mass concentration can possibly explain the result that the n values retrieved from this study lie above the midpoint of the range of previously reported values.

3.2. Atmospheric Implications.

For the measured refractive indices, a case study was formulated for a representative particle population of the central Amazon basin in the wet season.[41] During this time period, for clean conditions the submicrometer number-diameter distribution of the particle population is dominated by secondary organic material (i.e., 70−90% of submicrometer mass concentration).[42−44] For the case study, the number-diameter distribution $n(d)$ of Table 3 of Martin et al.[43] was taken. A Mie scattering algorithm[45] using $m(\lambda)$ of the present study was used to calculate the extinction efficiency Q_{ext} and the scattering efficiency Q_{sca} of each particle diameter d. Effective extinction efficiency was used for the particle population, as follows:

$$Q_{ext}^{eff}(m, \lambda) = \frac{\int_0^\infty d^2 Q_{ext}(d; m, \lambda) n(d) \mathrm{d}d}{\int_0^\infty d^2 n(d) \mathrm{d}d} \quad (2)$$

The effective single-scattering albedo ω^{eff} was calculated as follows:

$$\omega^{eff}(m, \lambda) = \frac{\int_0^\infty d^2 Q_{sca}(d; m, \lambda) n(d) \mathrm{d}d}{\int_0^\infty d^2 Q_{ext}(d; m, \lambda) n(d) \mathrm{d}d} \quad (3)$$

For comparison, in addition to using $m(\lambda)$ of the present study, calculations of Q_{ext}^{eff} and ω^{eff} using the refractive indices of organic carbon as prescribed in several atmospheric models were also performed.[46,47]

The ω^{eff} values of the SOMs decreased in the case study below unity (i.e., became absorptive) below a threshold wavelength (Figure 4a). This effect arises because the absorptive component of the refractive indices becomes significant below the threshold wavelength (Figure 3b). For monoterpene-derived SOM, the threshold value was near 400 nm, indicating weak light absorption in the UV and nearly completely reflective in the visible. For catechol-derived SOM, the threshold value was near 500 nm (i.e., in the middle of the visible portion of the spectrum). These results suggest that atmospheric SOM can have highly variable, wavelength-dependent single-scattering albedos, both for visible and UV wavelengths. In the case study, the monoterpene-derived SOM might represent predominantly gas-phase production pathways[30] whereas catechol-derived SOM has been suggested as a surrogate for humic-like substances produced in the atmosphere by aqueous-phase chemistry in cloud hydrometeors.[11]

Variability in the UV absorptive properties of atmospheric particles can influence the photolysis rates of the photochemical reactions in the troposphere. For an urban case study,

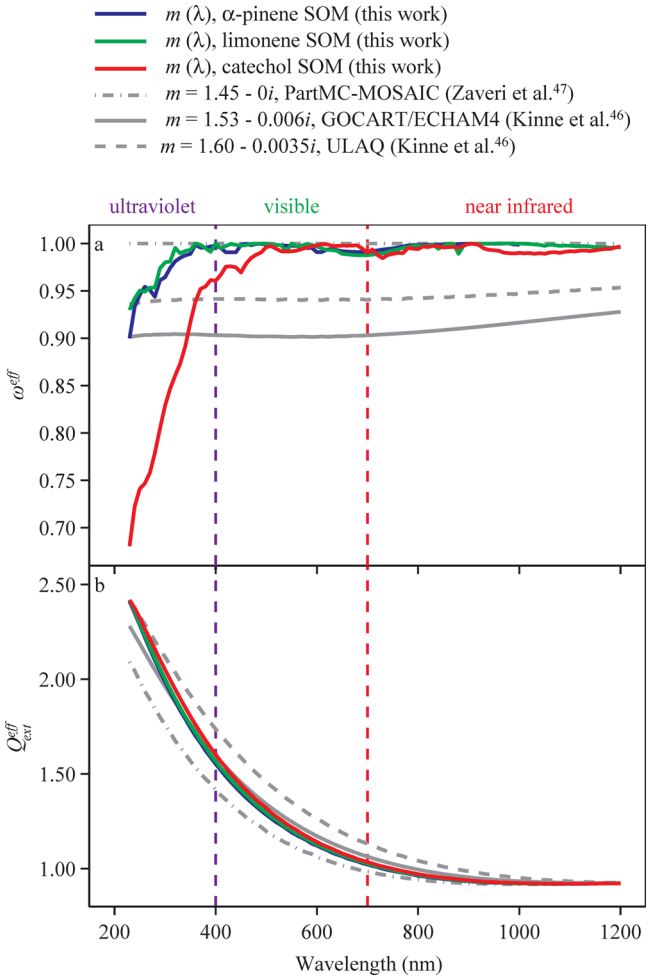

Figure 4. Modeled optical properties based on the results of this study for $m(\lambda)$ (Figure 3) and typical atmospheric particle populations. (a) Effective single-scattering albedo ω^{eff}. (b) Effective extinction efficiency Q^{eff}_{exit}. The optical properties are modeled for the particle number-diameter distribution measured during the Amazonian Aerosol Characterization Experiment (AMAZE-08).[43] Results based on optical constants reported in the literature are shown for comparison.

Dickerson et al.[3] showed that the dominance in the boundary layer of particles that scatter UV radiation (e.g., $\omega^{eff} = 0.96$) can accelerate the photochemical production of ozone whereas the presence of UV-absorbing particles (e.g., $\omega^{eff} = 0.75$) can inhibit ozone production. More generally, both in polluted and clean environments, the presence of scattering particles increased optical path length and thus accelerated photochemical cycles, at least in the upper part of the atmospheric mixed layer, whereas absorbing particles decreased the photon flux and thus slowed photochemical cycles.

Another important implication of variability in optical properties is the accuracy of AOD retrievals from satellite-based sensors and associated algorithms in the visible spectrum. The Q^{eff}_{ext} values modeled for the number-diameter distribution of the case study, however, were all similar (Figure 4b) because the different types of SOMs had similar real refractive indices in the visible (Figure 3a). The implication is that there is a characteristic curve for SOMs that does not depend on composition, at least for the studied SOMs. To the extent that this result holds generally, the retrieval of AOD from satellite-based observations is greatly simplified, and improved confidence is possible for the obtained values. Even so, by comparison to the measured uniformity of the studied SOMs, the real refractive indices actually used for organic carbon in several atmospheric models range from 1.45 to 1.60.[46,47] Our calculation suggests that this uncertainty leads to up to a 20% difference in calculated AOD in the UV/visible range (Figure 4b).

Another quantity retrieved by satellite analysis is the Angstrom exponent α of the atmospheric particle population, as a measure of the size distribution.[48] The Angstrom exponent from 310 to 550 nm in the present study was 0.85 for all three SOMs using the number-diameter distribution of the case study. In comparison, the Angstrom exponent calculated for the refractive indices in several atmospheric models without considering their wavelength dependence in the UV/visible ranges from 0.74 to 0.75. The possible implication is up to a 6% systematic error using the assumed refractive indices in place of the ones measured herein for the SOMs. A 6% error can imply an error of 12 nm in the mode distribution of the retrieved particles (i.e., on a base value of 142 nm for $\alpha = 0.85$).

In conclusion, the study presented here provides spectroscopic data of complex refractive index of different types of SOMs. This data set can improve the representation of SOM in optical databases of aerosol particles used for modeling and satellite studies. Furthermore, there is variability among different types of SOM with respect to absorption of UV radiation, with the implication of distinct effects on accelerating or slowing photochemical reaction cycles. Future laboratory work should assess the influence of atmospheric oxidation and other aging processes on refractive indices and further explore how the complex refractive indices of different types of SOM are related to chemical factors. Further atmospheric observations are needed for linking the properties of laboratory-generated SOM to that of the atmospheric SOM.

■ ASSOCIATED CONTENT

Supporting Information

Method validations using squalane and nigrosin dye. Tabulated data of complex refractive indices for different types of secondary organic material. This material is available free of charge via the Internet at http://pubs.acs.org.

■ AUTHOR INFORMATION

Corresponding Author

*E-mail: scot_martin@harvard.edu. Homepage: http://www.seas.harvard.edu/environmental-chemistry.

Notes

The authors declare no competing financial interest.

■ ACKNOWLEDGMENTS

This research was funded under NASA grant #NNX12AG95G through the NASA Radiation Science Program. This work was performed in part at the Harvard Center for Nanoscale Systems (CNS), a member of the NSF National Nanotechnology Infrastructure Network (NNIN). We acknowledge Jiangdong Deng and Jason Tresback from CNS for assistance with experiments. We thank Lindsay Renbaum-Wolff, Kelly Chance, Xiong Liu, Mikinori Kuwata, and Qi Chen for fruitful discussions.

REFERENCES

(1) Kaufman, Y. J.; Tanre, D.; Boucher, O. A Satellite View of Aerosols in the Climate System. *Nature* **2002**, *419*, 215−223.

(2) Bellouin, N.; Boucher, O.; Haywood, J.; Reddy, M. S. Global Estimate of Aerosol Direct Radiative Forcing from Satellite Measurements. *Nature* **2005**, *438*, 1138−1141.

(3) Dickerson, R. R.; Kondragunta, S.; Stenchikov, G.; Civerolo, K. L.; Doddridge, B. G.; Holben, B. N. The Impact of Aerosols on Solar Ultraviolet Radiation and Photochemical Smog. *Science* **1997**, *278*, 827−830.

(4) Remer, L. A.; et al. The MODIS Aerosol Algorithm, Products, and Validation. *J. Atmos. Sci.* **2005**, *62*, 947−973.

(5) Torres, O.; Tanskanen, A.; Veihelmann, B.; Ahn, C.; Braak, R.; Bhartia, P. K.; Veefkind, P.; Levelt, P. Aerosols and Surface UV Products from Ozone Monitoring Instrument Observations: An Overview. *J. Geophys. Res.* **2007**, *112*, D24S47.

(6) Hess, M.; Koepke, P.; Schult, I. Optical Properties of Aerosols and Clouds: The Software Package OPAC. *Bull. Amer. Meteorol. Soc.* **1998**, *79*, 831−844.

(7) Hallquist, M.; et al. The Formation, Properties and Impact of Secondary Organic Aerosol: Current and Emerging Issues. *Atmos. Chem. Phys.* **2009**, *9*, 5155−5236.

(8) Scott, C. E.; Rap, A.; Spracklen, D. V.; Forster, P. M.; Carslaw, K. S.; Mann, G. W.; Pringle, K. J.; Kivekäs, N.; Kulmala, M.; Lihavainen, H.; Tunved, P. The Direct and Indirect Radiative Effects of Biogenic Secondary Organic Aerosol. *Atmos. Chem. Phys. Discuss.* **2013**, *13*, 16961−17019.

(9) Ming, Y.; Ramaswamy, V.; Ginoux, P. A.; Horowitz, L. H. Direct Radiative Forcing of Anthropogenic Organic Aerosol. *J. Geophys. Res.* **2005**, *110*, D20208.

(10) Kim, H.; Barkey, B.; Paulson, S. E. Real Refractive Indices of Alpha- And Beta-Pinene and Toluene Secondary Organic Aerosols Generated from Ozonolysis and Photo-Oxidation. *J. Geophys. Res.* **2010**, *115*, D24212.

(11) Ofner, J.; Kruger, H. U.; Grothe, H.; Schmitt-Kopplin, P.; Whitmore, K.; Zetzsch, C. Physico-chemical Characterization of SOA Derived from Catechol and Guaiacol - A Model Substance for the Aromatic Fraction of Atmospheric HULIS. *Atmos. Chem. Phys.* **2011**, *11*, 1−15.

(12) Shapiro, E. L.; Szprengiel, J.; Sareen, N.; Jen, C. N.; Giordano, M. R.; McNeill, V. F. Light-absorbing Secondary Organic Material Formed by Glyoxal in Aqueous Aerosol Mimics. *Atmos. Chem. Phys.* **2009**, *9*, 2289−2300.

(13) Updyke, K. M.; Nguyen, T. B.; Nizkorodov, S. A. Formation of Brown Carbon via Reactions of Ammonia with Secondary Organic Aerosols from Biogenic and Anthropogenic Precursors. *Atmos. Environ.* **2012**, *63*, 22−31.

(14) Jacobson, M. Z. Isolating Nitrated and Aromatic Aerosols and Nitrated Aromatic Gases As Sources of Ultraviolet Light Absorption. *J. Geophys. Res.* **1999**, *104*, 3527−3542.

(15) Laskin, J.; Laskin, A.; Roach, P. J.; Slysz, G. W.; Anderson, G. A.; Nizkorodov, S. A.; Bones, D. L.; Nguyen, L. Q. High-Resolution Desorption Electrospray Ionization Mass Spectrometry for Chemical Characterization of Organic Aerosols. *Anal. Chem.* **2010**, *82*, 2048−2058.

(16) Hoffer, A.; Gelencsér, A.; Guyon, P.; Kiss, G.; Schmid, O.; Frank, G. P.; Artaxo, P.; Andreae, M. O. Optical Properties of Humic-Like Substances (HULIS) in Biomass-Burning Aerosols. *Atmos. Chem. Phys.* **2006**, *6*, 3563−3570.

(17) Kirchstetter, T. W.; Novakov, T.; Hobbs, P. V. Evidence that the Spectral Dependence of Light Absorption by Aerosols Is Affected by Organic Carbon. *J. Geophys. Res.* **2004**, *109*, D21208.

(18) Andreae, M. O.; Gelencser, A. Black Carbon or Brown Carbon? The Nature of Light-Absorbing Carbonaceous Aerosols. *Atmos. Chem. Phys.* **2006**, *6*, 3131−3148.

(19) Zhong, M.; Jang, M. Light Absorption Coefficient Measurement of SOA using a UV−Visible Spectrometer Connected with an Integrating Sphere. *Atmos. Environ.* **2011**, *45*, 4263−4271.

(20) Lambe, A. T.; Cappa, C. D.; Massoli, P.; Onasch, T. B.; Forestieri, S. D.; Martin, A. T.; Cummings, M. J.; Croasdale, D. R.; Brune, W. H.; Worsnop, D. R.; Davidovits, P. Relationship between Oxidation Level and Optical Properties of Secondary Organic Aerosol. *Environ. Sci. Technol.* **2013**, *47*, 6349−6357.

(21) Kim, H.; Paulson, S. E. Real Refractive Indices and Volatility of Secondary Organic Aerosol Generated from Photooxidation and Ozonolysis of Limonene, α-Pinene and Toluene. *Atmos. Chem. Phys.* **2013**, *13*, 7711−7723.

(22) Nakayama, T.; Matsumi, Y.; Sato, K.; Imamura, T.; Yamazaki, A.; Uchiyama, A. Laboratory Studies on Optical Properties of Secondary Organic Aerosols Generated during the Photooxidation of Toluene and the Ozonolysis of Alpha-Pinene. *J. Geophys. Res.* **2010**, *115*, D24204.

(23) Nakayama, T.; Sato, K.; Matsumi, Y.; Imamura, T.; Yamazaki, A.; Uchiyama, A. Wavelength Dependence of Refractive Index of Secondary Organic Aerosols Generated during the Ozonolysis and Photooxidation of α-Pinene. *SOLA* **2012**, *8*, 119−123.

(24) Nakayama, T.; Sato, K.; Matsumi, Y.; Imamura, T.; Yamazaki, A.; Uchiyama, A. Wavelength and NOx Dependent Complex Refractive Index of SOAs Generated from the Photooxidation of Toluene. *Atmos. Chem. Phys.* **2013**, *13*, 531−545.

(25) Redmond, H.; Thompson, J. E. Evaluation of a Quantitative Structure-Property Relationship (QSPR) for Predicting Mid-Visible Refractive Index of Secondary Organic Aerosol (SOA). *Phys. Chem. Chem. Phys.* **2011**, *13*, 6872−6882.

(26) Fujiwara, H., *Spectroscopic ellipsometry: principles and applications*. Wiley: 2007.

(27) Tammer, M.; Monkman, A. P. Measurement of the Anisotropic Refractive Indices of Spin Cast Thin Poly(2-methoxy-5-(2′-ethylhexyloxy)-p-phenylenevinylene) (MEH−PPV) Films. *Adv. Mater.* **2002**, *14*, 210−212.

(28) Ramsdale, C. M.; Greenham, N. C. Ellipsometric Determination of Anisotropic Optical Constants in Electroluminescent Conjugated Polymers. *Adv. Mater.* **2002**, *14*, 212−215.

(29) McNeill, V. F.; Loerting, T.; Geiger, F. M.; Trout, B. L.; Molina, M. J. Hydrogen Chloride-Induced Surface Disordering on Ice. *Proc. Natl. Acad. Sci.* **2006**, *103*, 9422−9427.

(30) Kanakidou, M.; et al. Organic Aerosol and Global Climate Modelling: A Review. *Atmos. Chem. Phys.* **2005**, *5*, 1053−1123.

(31) Shrestha, M.; Zhang, Y.; Ebben, C. J.; Martin, S. T.; Geiger, F. M. Vibrational Sum Frequency Generation Spectroscopy of Secondary Organic Material Produced by Condensational Growth from α-Pinene Ozonolysis. *J. Phys. Chem. A* **2013**, *117*, 8427−8436.

(32) Liu, Y. J.; Herdlinger-Blatt, I.; McKinney, K. A.; Martin, S. T. Production of Methyl Vinyl Ketone and Methacrolein via the Hydroperoxyl Pathway of Isoprene Oxidation. *Atmos. Chem. Phys.* **2013**, *13*, 5715−5730.

(33) Dixkens, J.; Fissan, H. Development of an Electrostatic Precipitator for off-Line Particle Analysis. *Aerosol Sci. Technol.* **1999**, *30*, 438−453.

(34) *Guide to Using WVASE32: Software for Spectroscopic Ellipsometry Data Acquisition and Analysis*; J.A. Woollam Co., Inc., 2008.

(35) Kuwata, M.; Zorn, S. R.; Martin, S. T. Using Elemental Ratios to Predict the Density of Organic Material Composed of Carbon, Hydrogen, and Oxygen. *Environ. Sci. Technol.* **2012**, *46*, 787−794.

(36) Chen, Q.; Liu, Y.; Donahue, N. M.; Shilling, J. E.; Martin, S. T. Particle-phase Chemistry of Secondary Organic Material: Modeled Compared to Measured O:C and H:C Elemental Ratios Provide Constraints. *Environ. Sci. Technol.* **2011**, *45*, 4763−4770.

(37) Yang, C.-J.; Jenekhe, S. A. Group Contribution to Molar Refraction and Refractive Index of Conjugated Polymers. *Chem. Mater.* **1995**, *7*, 1276−1285.

(38) Jenkins, F.; White, H., *Fundamentals of optics*, fourth ed.; McGraw-Hill Higher Education: New York, 1976.

(39) Toole, J. R.; Renbaum-Wolff, L.; Smith, G. D. A Calibration Technique for Improving Refractive Index Retrieval from Aerosol Cavity Ring-Down Spectroscopy. *Aerosol Sci. Technol.* **2013**, *47*, 955−965.

(40) Shilling, J. E.; Chen, Q.; King, S. M.; Rosenoern, T.; Kroll, J. H.; Worsnop, D. R.; DeCarlo, P. F.; Aiken, A. C.; Sueper, D.; Jimenez, J. L.; Martin, S. T. Loading-dependent Elemental Composition of Alpha-Pinene SOA Particles. *Atmos. Chem. Phys.* **2009**, *9*, 771−782.
(41) Martin, S. T.; et al. Sources and Properties of Amazonian Aerosol Particles. *Rev. Geophys.* **2010**, *48*, RG2002.
(42) Chen, Q.; et al. Mass Spectral Characterization of Submicron Biogenic Organic Particles in the Amazon Basin. *Geophys. Res. Lett.* **2009**, *36*, L20806.
(43) Martin, S. T.; et al. An Overview of the Amazonian Aerosol Characterization Experiment 2008 (AMAZE-08). *Atmos. Chem. Phys.* **2010**, *10*, 11415−11438.
(44) Pöschl, U.; et al. Rainforest Aerosols As Biogenic Nuclei of Clouds and Precipitation in the Amazon. *Science* **2010**, *329*, 1513−1516.
(45) Bohren, C. F.; Huffman, D. R. *Absorption and Scattering of Light by Small Particles*; Wiley: New York, 1983; p 530.
(46) Kinne, S.; et al. Monthly Averages of Aerosol Properties: A Global Comparison among Models, Satellite Data, and AERONET Ground Data. *J. Geophys. Res.* **2003**, *108*, 4634.
(47) Zaveri, R. A.; Barnard, J. C.; Easter, R. C.; Riemer, N.; West, M. Particle-resolved Simulation of Aerosol Size, Composition, Mixing State, and the Associated Optical and Cloud Condensation Nuclei Activation Properties in an Evolving Urban Plume. *J. Geophys. Res.* **2010**, *115*, D17210.
(48) Schuster, G. L.; Dubovik, O.; Holben, B. N. Angstrom Exponent and Bimodal Aerosol Size Distributions. *J. Geophys. Res.* **2006**, *111*, D07207.

Supporting Information

Complex Refractive Indices of Thin Films of Secondary Organic Materials by Spectroscopic Ellipsometry from 220 to 1200 nm

Pengfei Liu (1), Yue Zhang (1), and Scot T. Martin* (1, 2)

(1) School of Engineering and Applied Sciences, Harvard University, Cambridge, Massachusetts, USA, 02138

(2) Department of Earth and Planetary Sciences, Harvard University, Cambridge, Massachusetts, USA, 02138

E-mail: scot_martin@harvard.edu

http://www.seas.harvard.edu/environmental-chemistry

*To Whom Correspondence Should be Addressed

The following supporting information contains 12 pages and includes 2 figures and 1 table.

S1 Method validation

S1.1 Validation using squalane (non-absorbing standard)

Squalane (CAS#: 111-01-3, Sigma Aldrich, 99%) was used as a non-absorbing standard for method validation. Squalane is a low volatility liquid (vapor pressure of 10^{-7} Torr at room temperature[1]) that is stable in air at room temperature. A previous study reported zero values of imaginary part of refractive index *k* for squalane in the ultraviolet and visible regions for $\lambda > 200$ nm.[2] The real refractive index *n* has been measured using different techniques.[2-4] In a recent study, squalane was chosen as a calibration standard for cavity ring-down aerosol spectroscopy (CRD-AS).[5]

Similar to the synthesis of SOM thin films, the squalane thin film was produced by electrostatic precipitation of particles onto a silicon substrate using an electrostatic precipitator (TSI 3089). The method for squalane particle generation was similar to that described in Toole et al.[5] Pure squalane liquid was aerosolized by a disposable nebulizer (Hudson RCI, MICRO MIST nebulizer) with 1.50 sLpm (standard liters per minute) of pure air controlled by a mass flow controller. The aerosol flow was diluted with a 1.0 sLpm pure air flow in a mixing bottle and then drawn through a bipolar charger (TSI 3077) by the electrostatic precipitator at a flow rate of 1.50 sLpm. The synthesized squalane thin film was optically reflective.

The spectroscopic ellipsometry measurement for squalane thin film was similar to that described in section 2.3 for SOM samples. Based on literature[2], the *k* values were set to be zero in studied spectral region (310-700 nm) in the data analysis. The *n* values were obtained from two different fitting methods using *WVASE32* software: (1) point-by-point fitting, which fits *n* value at each measured wavelength and (2) Cauchy model fitting, which assumes that the wavelength dependence of *n* follows Cauchy dispersion relation (see Eq. 1 in main text). Data

analysis showed that the thickness of the squalane thin film was 40 nm, with non-uniformity of 15%. The *n* values from different fitting methods are in good agreement (Fig. S1). The absolute differences of *n* are smaller than 0.006. Literature data are also shown in Fig. S1 for comparison.

The *n* values of squalane obtained from this study agree well with literature data. For example, at λ = 355 nm, our results suggest values of n = 1.470 (±0.010) from point-by-point fitting and 1.472 (±0.008) from Cauchy fitting. In comparison, Toole[3] measured a value n = 1.471 at λ = 355 nm from bulk liquid measurement using a Snell's law cell. The ellipsometry measurement (J.A. Woollam, model M2000) conducted in J.A. Woollam laboratories suggested n = 1.471[3]. Painter et al.[2] reported n = 1.472 from reflectance measurement. The comparison validates the refractive index from ellipsometry measurement of thin films synthesized from electrostatic precipitation.

S1.2 Validation using nigrosin dye (light-absorbing standard)

Nigrosin (CAS#: 8005-03-6, acid black 2, Sigma Aldrich) is a water soluble dye that has been used in previous studies to generate absorbing particles for aerosol instrument validations.[6-8] Nigrosin has strong absorption in the UV and visible regions. Its water solution is dark blue. A complex refractive index value of nigrosin $m = 1.67 - 0.26i$ was measured in bulk form for 632.8 nm light.[9] Two CRD-AS measurements reported values of $m = 1.70 - 0.31i$[7] and $m = 1.649 - 0.238i$[8] respectively at 532 nm wavelength for nigrosin in particle form.

In the present study, two nigrosin thin film samples were synthesized from spin coating of a 1.0 wt% nigrosin water solution onto silicon substrates. The film thicknesses of the two samples determined from ellipsometry measurements were 14 nm and 11 nm, respectively. The complex refractive indices retrieved by spectroscopic ellipsometry from 220 to 700 nm are shown in Fig. S2. We also attempted to deposit atomized nigrosin particles onto a silicon

substrate using electrostatic precipitation. This method, however, formed micron-sized aggregated particles on the substrate instead of a reflective thin film and could not be used for ellipsometry measurement.

In addition to ellipsometry measurement of spin-coated nigrosin films, the UV-visible absorption spectrum of a water solution that contains 0.001 wt% nigrosin was measured by UV-visible spectrophotometry (Agilent, model 8453). The wavelength-dependent $k(\lambda)$ values can be calculated from the base-10 absorbance $A(\lambda)$ of a nigrosin solution with mass concentration c (g L^{-1}) measured over optical pathlength L (cm):[10]

$$k(\lambda) = 1000 \ln(10) \frac{A \cdot \rho \cdot \lambda}{4\pi \cdot c \cdot l} \quad \text{(S1)}$$

In this calculation, the material density ρ of nigrosin was taken as 1.5 g cm^{-3} (no literature data available). The calculated $k(\lambda)$ are shown in Fig. S2b for comparison.

Figure S2 shows that both $n(\lambda)$ and $k(\lambda)$ retrieved from ellipsometry measurements are in good agreement with literature data. The interpolation of ellipsometry data reported a value of m = 1.61 (±0.01) - 0.23 (±0.01)i at 532 nm, which supported the CRD-AS measurements of nigrosin particles from Lack et al.[7] (1.70 - 0.31i) and Dinar et al.[8] (1.649 - 0.238i). The interpolated value m = 1.73 (±0.02) - 0.27 (±0.02)i from ellipsometry data at 632.8 nm also agrees well with bulk form measurement from Pinnick et al.[9] The wavelength dependence of $k(\lambda)$ was confirmed by the absorption measurement of nigrosin water solution using a UV-visible spectrophotometer.

The validation experiments of S1.1 and S1.2 confirmed the applicability of the thin film ellipsometry measurements.

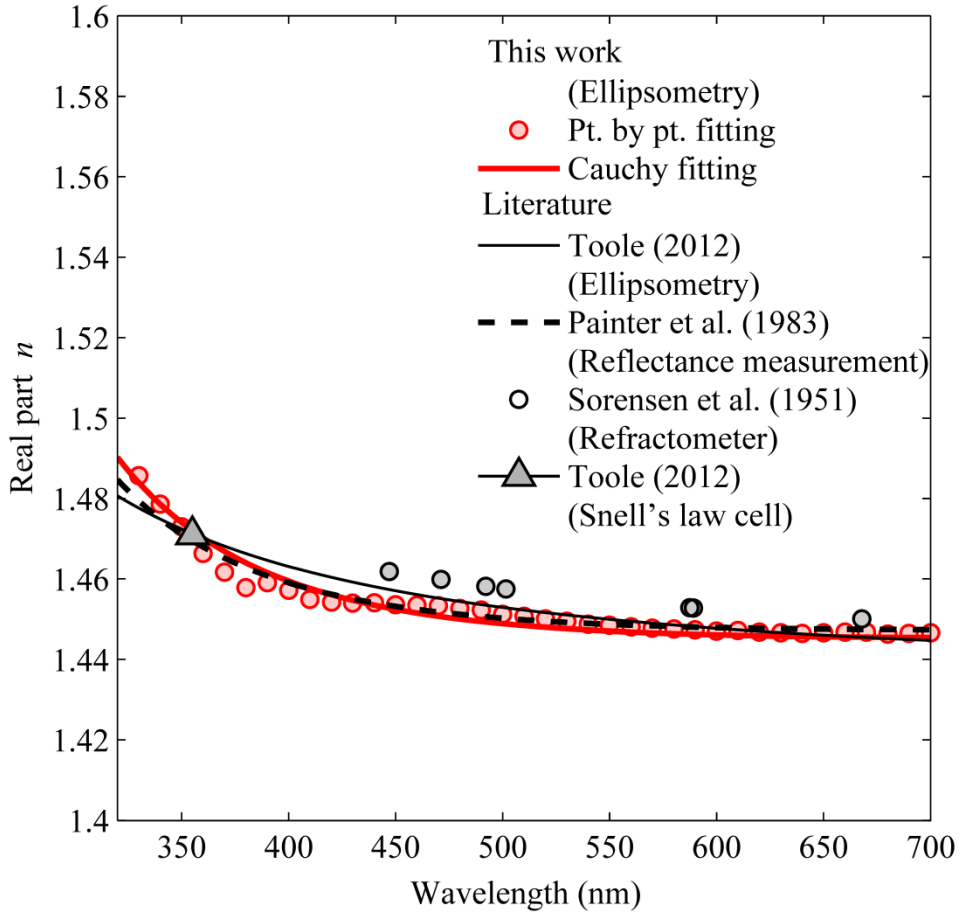

Figure S1. Wavelength-dependent real refractive indices $n(\lambda)$ for squalane. Results from literature are shown for comparison.

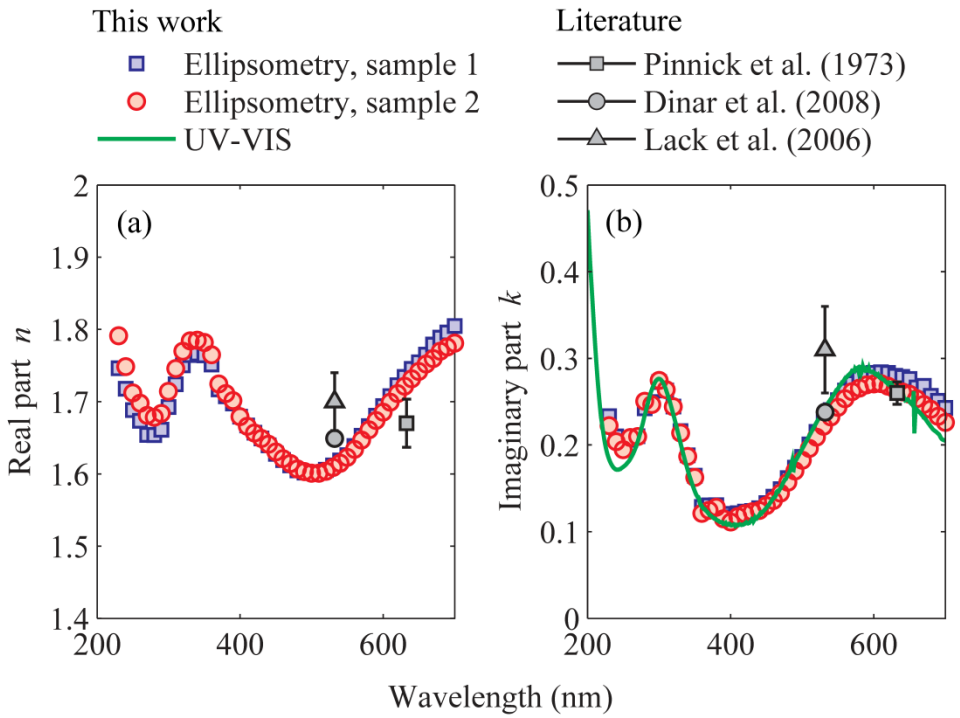

Figure S2. Wavelength-dependent complex refractive indices $m(\lambda)$ for nigrosin. Results for literature are shown for comparison.

Table S1. Wavelength-dependent complex refractive indices $m(\lambda) = n - i\,k$ for different types of secondary organic material.

SOM type:	α-pinene ozonolysis		limonene ozonolysis		catechol ozonolysis	
wavelength (nm)	*n*	*k*	*n*	*k*	*n*	*k*
220	1.6129	0.0088	1.6152	0.0050		
225	1.6050	0.0069	1.6079	0.0041		
230	1.5978	0.0065	1.6011	0.0039	1.6374	0.0678
235	1.5912	0.0055	1.5950	0.0036	1.6301	0.0558
240	1.5852	0.0037	1.5893	0.0031	1.6234	0.0477
245	1.5797	0.0032	1.5841	0.0029	1.6171	0.0422
250	1.5746	0.0029	1.5792	0.0026	1.6113	0.0402
255	1.5699	0.0026	1.5747	0.0024	1.6059	0.0391
260	1.5656	0.0024	1.5706	0.0027	1.6009	0.0378
265	1.5615	0.0022	1.5668	0.0027	1.5962	0.0365
270	1.5578	0.0026	1.5632	0.0024	1.5918	0.0335
275	1.5544	0.0028	1.5598	0.0024	1.5877	0.0303
280	1.5511	0.0030	1.5567	0.0024	1.5839	0.0270
285	1.5481	0.0026	1.5538	0.0018	1.5803	0.0239
290	1.5453	0.0020	1.5511	0.0013	1.5769	0.0205
295	1.5427	0.0019	1.5485	0.0012	1.5737	0.0180
300	1.5403	0.0018	1.5461	0.0009	1.5707	0.0157
305	1.5380	0.0015	1.5439	0.0008	1.5679	0.0139
310	1.5358	0.0012	1.5418	0.0009	1.5652	0.0129
315	1.5338	0.0011	1.5398	0.0007	1.5627	0.0118
320	1.5319	0.0009	1.5379	0.0002	1.5603	0.0108
325	1.5301	0.0008	1.5361	0.0004	1.5580	0.0101
330	1.5284	0.0007	1.5344	0.0005	1.5558	0.0093
335	1.5267	0.0006	1.5328	0.0003	1.5538	0.0088
340	1.5252	0.0006	1.5313	0.0003	1.5519	0.0073
345	1.5238	0.0007	1.5299	0.0004	1.5500	0.0059
350	1.5224	0.0005	1.5285	0.0003	1.5483	0.0051
355	1.5211	0.0002	1.5272	0.0001	1.5466	0.0042
360	1.5199	0.0001	1.5260	0.0000	1.5450	0.0034
365	1.5188	0.0001	1.5248	0.0000	1.5435	0.0028
370	1.5177	0.0002	1.5237	0.0001	1.5420	0.0026
375	1.5166	0.0003	1.5227	0.0000	1.5407	0.0027
380	1.5156	0.0002	1.5217	0.0002	1.5393	0.0024
385	1.5146	0.0002	1.5207	0.0002	1.5381	0.0021
390	1.5137	0.0001	1.5198	0.0004	1.5368	0.0020
395	1.5129	0.0001	1.5189	0.0003	1.5357	0.0020
400	1.5120	0.0001	1.5180	0.0000	1.5346	0.0020

405	1.5112	0.0001	1.5172	0.0001	1.5335	0.0019
410	1.5105	0.0002	1.5165	0.0002	1.5325	0.0016
415	1.5098	0.0003	1.5157	0.0002	1.5315	0.0014
420	1.5091	0.0004	1.5150	0.0001	1.5305	0.0012
425	1.5084	0.0003	1.5143	0.0001	1.5296	0.0012
430	1.5077	0.0004	1.5137	0.0000	1.5287	0.0012
435	1.5071	0.0005	1.5130	0.0000	1.5279	0.0013
440	1.5065	0.0004	1.5124	0.0001	1.5271	0.0012
445	1.5060	0.0002	1.5118	0.0001	1.5263	0.0015
450	1.5054	0.0001	1.5113	0.0001	1.5255	0.0015
455	1.5049	0.0000	1.5107	0.0001	1.5248	0.0012
460	1.5044	0.0000	1.5102	0.0001	1.5241	0.0010
465	1.5039	0.0000	1.5097	0.0000	1.5234	0.0008
470	1.5034	0.0001	1.5092	0.0000	1.5228	0.0007
475	1.5030	0.0000	1.5088	0.0000	1.5221	0.0006
480	1.5026	0.0000	1.5083	0.0000	1.5215	0.0006
485	1.5021	0.0000	1.5079	0.0000	1.5209	0.0006
490	1.5017	0.0000	1.5074	0.0000	1.5204	0.0004
495	1.5013	0.0000	1.5070	0.0000	1.5198	0.0002
500	1.5010	0.0000	1.5066	0.0000	1.5193	0.0001
505	1.5006	0.0000	1.5063	0.0000	1.5188	0.0001
510	1.5002	0.0001	1.5059	0.0001	1.5183	0.0001
515	1.4999	0.0001	1.5055	0.0000	1.5178	0.0002
520	1.4996	0.0001	1.5052	0.0001	1.5173	0.0003
525	1.4993	0.0001	1.5049	0.0000	1.5168	0.0003
530	1.4990	0.0001	1.5045	0.0001	1.5164	0.0004
535	1.4987	0.0001	1.5042	0.0005	1.5160	0.0004
540	1.4984	0.0001	1.5039	0.0004	1.5155	0.0004
545	1.4981	0.0001	1.5036	0.0003	1.5151	0.0004
550	1.4978	0.0001	1.5033	0.0000	1.5147	0.0004
555	1.4975	0.0001	1.5031	0.0001	1.5144	0.0004
560	1.4973	0.0001	1.5028	0.0001	1.5140	0.0003
565	1.4970	0.0001	1.5025	0.0001	1.5136	0.0003
570	1.4968	0.0002	1.5023	0.0001	1.5133	0.0003
575	1.4966	0.0002	1.5020	0.0001	1.5129	0.0002
580	1.4963	0.0002	1.5018	0.0000	1.5126	0.0002
585	1.4961	0.0002	1.5015	0.0000	1.5123	0.0002
590	1.4959	0.0002	1.5013	0.0001	1.5120	0.0001
595	1.4957	0.0003	1.5011	0.0001	1.5116	0.0001
600	1.4955	0.0004	1.5009	0.0002	1.5113	0.0001
605	1.4953	0.0004	1.5007	0.0002	1.5111	0.0000
610	1.4951	0.0004	1.5005	0.0002	1.5108	0.0000
615	1.4949	0.0003	1.5003	0.0003	1.5105	0.0000
620	1.4947	0.0003	1.5001	0.0003	1.5102	0.0000
625	1.4945	0.0003	1.4999	0.0003	1.5100	0.0001

630	1.4944	0.0003	1.4997	0.0003	1.5097	0.0001
635	1.4942	0.0003	1.4995	0.0003	1.5095	0.0001
640	1.4940	0.0003	1.4994	0.0004	1.5092	0.0001
645	1.4939	0.0003	1.4992	0.0004	1.5090	0.0001
650	1.4937	0.0004	1.4990	0.0005	1.5087	0.0001
655	1.4936	0.0004	1.4989	0.0005	1.5085	0.0001
660	1.4934	0.0004	1.4987	0.0006	1.5083	0.0001
665	1.4933	0.0004	1.4985	0.0006	1.5081	0.0001
670	1.4931	0.0004	1.4984	0.0006	1.5079	0.0001
675	1.4930	0.0004	1.4982	0.0006	1.5077	0.0001
680	1.4929	0.0004	1.4981	0.0006	1.5075	0.0001
685	1.4927	0.0004	1.4980	0.0006	1.5073	0.0001
690	1.4926	0.0004	1.4978	0.0006	1.5071	0.0003
695	1.4925	0.0004	1.4977	0.0006	1.5069	0.0004
700	1.4924	0.0004	1.4976	0.0006	1.5067	0.0005
705	1.4922	0.0004	1.4974	0.0006	1.5065	0.0004
710	1.4921	0.0004	1.4973	0.0006	1.5063	0.0003
715	1.4920	0.0004	1.4972	0.0006	1.5062	0.0004
720	1.4919	0.0003	1.4971	0.0005	1.5060	0.0006
725	1.4918	0.0003	1.4969	0.0005	1.5058	0.0007
730	1.4917	0.0003	1.4968	0.0005	1.5057	0.0008
735	1.4916	0.0003	1.4967	0.0005	1.5055	0.0007
740	1.4915	0.0003	1.4966	0.0005	1.5054	0.0006
745	1.4914	0.0003	1.4965	0.0004	1.5052	0.0006
750	1.4913	0.0002	1.4964	0.0004	1.5051	0.0005
755	1.4912	0.0002	1.4963	0.0004	1.5049	0.0005
760	1.4911	0.0002	1.4962	0.0003	1.5048	0.0005
765	1.4910	0.0002	1.4961	0.0003	1.5046	0.0007
770	1.4909	0.0002	1.4960	0.0002	1.5045	0.0005
775	1.4908	0.0001	1.4959	0.0002	1.5044	0.0004
780	1.4907	0.0001	1.4958	0.0002	1.5042	0.0003
785	1.4906	0.0001	1.4957	0.0002	1.5041	0.0002
790	1.4906	0.0001	1.4956	0.0001	1.5040	0.0003
795	1.4905	0.0001	1.4955	0.0001	1.5039	0.0003
800	1.4904	0.0001	1.4955	0.0001	1.5037	0.0003
805	1.4903	0.0001	1.4954	0.0001	1.5036	0.0002
810	1.4903	0.0001	1.4953	0.0001	1.5035	0.0002
815	1.4902	0.0001	1.4952	0.0001	1.5034	0.0002
820	1.4901	0.0001	1.4951	0.0001	1.5033	0.0002
825	1.4900	0.0001	1.4950	0.0001	1.5032	0.0001
830	1.4900	0.0001	1.4950	0.0000	1.5031	0.0001
835	1.4899	0.0001	1.4949	0.0001	1.5029	0.0002
840	1.4898	0.0000	1.4948	0.0003	1.5028	0.0001
845	1.4898	0.0000	1.4948	0.0001	1.5027	0.0002
850	1.4897	0.0001	1.4947	0.0001	1.5026	0.0002

855	1.4896	0.0000	1.4946	0.0001	1.5025	0.0002
860	1.4896	0.0000	1.4945	0.0000	1.5024	0.0002
865	1.4895	0.0000	1.4945	0.0000	1.5023	0.0002
870	1.4894	0.0000	1.4944	0.0000	1.5023	0.0002
875	1.4894	0.0000	1.4943	0.0002	1.5022	0.0002
880	1.4893	0.0000	1.4943	0.0006	1.5021	0.0002
885	1.4893	0.0000	1.4942	0.0004	1.5020	0.0001
890	1.4892	0.0000	1.4942	0.0001	1.5019	0.0001
895	1.4892	0.0000	1.4941	0.0001	1.5018	0.0001
900	1.4891	0.0000	1.4940	0.0000	1.5017	0.0000
905	1.4890	0.0000	1.4940	0.0000	1.5016	0.0001
910	1.4890	0.0000	1.4939	0.0000	1.5016	0.0000
915	1.4889	0.0000	1.4939	0.0000	1.5015	0.0003
920	1.4889	0.0000	1.4938	0.0000	1.5014	0.0001
925	1.4888	0.0000	1.4938	0.0000	1.5013	0.0002
930	1.4888	0.0000	1.4937	0.0000	1.5012	0.0003
935	1.4887	0.0000	1.4937	0.0000	1.5012	0.0003
940	1.4887	0.0000	1.4936	0.0000	1.5011	0.0004
945	1.4886	0.0000	1.4935	0.0000	1.5010	0.0004
950	1.4886	0.0000	1.4935	0.0000	1.5010	0.0004
955	1.4886	0.0000	1.4935	0.0000	1.5009	0.0004
960	1.4885	0.0000	1.4934	0.0000	1.5008	0.0005
965	1.4885	0.0000	1.4934	0.0000	1.5007	0.0005
970	1.4884	0.0000	1.4933	0.0000	1.5007	0.0006
975	1.4884	0.0000	1.4933	0.0000	1.5006	0.0006
980	1.4883	0.0000	1.4932	0.0000	1.5006	0.0006
985	1.4883	0.0000	1.4932	0.0000	1.5005	0.0005
990	1.4883	0.0001	1.4931	0.0000	1.5004	0.0007
995	1.4882	0.0001	1.4931	0.0000	1.5004	0.0006
1000	1.4882	0.0001	1.4930	0.0000	1.5003	0.0006
1005			1.4930	0.0000	1.5002	0.0006
1010			1.4930	0.0000	1.5002	0.0006
1015			1.4929	0.0000	1.5001	0.0006
1020			1.4929	0.0000	1.5001	0.0006
1025			1.4928	0.0000	1.5000	0.0007
1030			1.4928	0.0001	1.5000	0.0007
1035			1.4928	0.0001	1.4999	0.0007
1040			1.4927	0.0001	1.4998	0.0007
1045			1.4927	0.0001	1.4998	0.0007
1050			1.4926	0.0002	1.4997	0.0007
1055			1.4926	0.0001	1.4997	0.0006
1060			1.4926	0.0001	1.4996	0.0006
1065			1.4925	0.0001	1.4996	0.0006
1070			1.4925	0.0001	1.4995	0.0006
1075			1.4925	0.0001	1.4995	0.0006

1080	1.4924	0.0002	1.4994	0.0007
1085	1.4924	0.0001	1.4994	0.0006
1090	1.4924	0.0001	1.4993	0.0006
1095	1.4923	0.0001	1.4993	0.0006
1100	1.4923	0.0002	1.4993	0.0006
1105	1.4923	0.0002	1.4992	0.0006
1110	1.4922	0.0002	1.4992	0.0006
1115	1.4922	0.0002	1.4991	0.0006
1120	1.4922	0.0002	1.4991	0.0005
1125	1.4922	0.0002	1.4990	0.0005
1130	1.4921	0.0002	1.4990	0.0005
1135	1.4921	0.0002	1.4990	0.0006
1140	1.4921	0.0002	1.4989	0.0006
1145	1.4920	0.0003	1.4989	0.0006
1150	1.4920	0.0003	1.4988	0.0005
1155	1.4920	0.0003	1.4988	0.0005
1160	1.4920	0.0002	1.4988	0.0004
1165	1.4919	0.0003	1.4987	0.0004
1170	1.4919	0.0003	1.4987	0.0004
1175	1.4919	0.0003	1.4986	0.0004
1180	1.4919	0.0003	1.4986	0.0004
1185	1.4918	0.0003	1.4986	0.0004
1190	1.4918	0.0003	1.4985	0.0003
1195	1.4918	0.0003	1.4985	0.0003
1200	1.4918	0.0003	1.4985	0.0002

References

(1) Köhler, S. P. K.; Allan, M.; Kelso, H.; Henderson, D. A.; McKendrick, K. G. The effects of surface temperature on the gas-liquid interfacial reaction dynamics of O(3P)+squalane. *The Journal of Chemical Physics* **2005,** *122*, 024712.

(2) Painter, L. R.; Attrey, J. S.; Hubbell, H. H.; Birkhoff, R. D. Vacuum ultraviolet optical properties of squalane and squalene. *Journal of Applied Physics* **1984,** *55*, 756-759.

(3) Toole, J. R. Reducing uncertainties in aerosol optical properties with cavity ring-down spectroscopy. University of Georgia, Athens, Georgia, 2012.

(4) Sörensen, N. A.; Gillebo, T.; Holtermann, H.; Sörensen, J. S. Studies related to pristane VI. synthesis of digeranyl with some remarks on the physical constants of crocetane. *Acta Chemica Scandinavica* **1951,** *5*, 757-765.

(5) Toole, J. R.; Renbaum-Wolff, L.; Smith, G. D. A Calibration Technique for Improving Refractive Index Retrieval from Aerosol Cavity Ring-Down Spectroscopy. *Aerosol Sci. Technol.* **2013,** *47*, 955-965.

(6) Bond, T. C.; Anderson, T. L.; Campbell, D. Calibration and Intercomparison of Filter-Based Measurements of Visible Light Absorption by Aerosols. *Aerosol Sci. Technol.* **1999,** *30*, 582-600.

(7) Lack, D. A.; Lovejoy, E. R.; Baynard, T.; Pettersson, A.; Ravishankara, A. R. Aerosol Absorption Measurement using Photoacoustic Spectroscopy: Sensitivity, Calibration, and Uncertainty Developments. *Aerosol Sci. Technol.* **2006,** *40*, 697-708.

(8) Dinar, E.; Abo Riziq, A.; Spindler, C.; Erlick, C.; Kiss, G.; Rudich, Y. The complex refractive index of atmospheric and model humic-like substances (HULIS) retrieved by a cavity ring down aerosol spectrometer (CRD-AS). *Faraday Discussions* **2008,** *137*, 279-295.

(9) Pinnick, R. G.; Rosen, J. M.; Hofmann, D. J. Measured Light-Scattering Properties of Individual Aerosol Particles Compared to Mie Scattering Theory. *Appl. Optics* **1973,** *12*, 37-41.

(10) Sun, H.; Biedermann, L.; Bond, T. C. Color of brown carbon: A model for ultraviolet and visible light absorption by organic carbon aerosol. *Geophys. Res. Lett.* **2007,** *34*, L17813.